Int Ophthalmol (2019) 39:2373–2383
https://doi.org/10.1007/s10792-019-01077-w

ORIGINAL PAPER

Analysis of pattern electroretinogram signals of early primary open-angle glaucoma in discrete wavelet transform coefficients domain

Homa Hassankarimi · Seyed Mohammad Reza Noori · Ebrahim Jafarzadehpour · Shahin Yazdani · Fatemeh Radinmehr

Received: 23 December 2017 / Accepted: 25 January 2019 / Published online: 6 February 2019

Abstract

Purpose To evaluate discrete wavelet transform coefficients and identify descriptors of pattern electroretinogram (PERG) waveforms in order to determine PERG characteristics for optimizing the diagnosis of early primary open-angle glaucoma (POAG).

Methods Pattern electroretinogram was performed in 30 normal eyes and 30 eyes with primary open-angle glaucoma according to the ISCEV protocol. The check size was 0.8° and 16°, and the color was black/white in both groups. The results were analyzed in time domain (TD) and discrete wavelet transform (DWT) using the MATLAB software. The mean value, standard deviation, and relative energy of level 6 and 7 detail coefficients (d6, d7) and level 7 approximation coefficients (a7) of Daubechies 4 (db4), Daubechies 8 (db8), Symlet 5 (sym5), Symlet 7 (sym7), and Coiflet 5 (coif5) wavelets were calculated. In all the mentioned wavelets, DWT descriptors

H. Hassankarimi
Department of Medical Physics, School of Medicine, Iran University of Medical Sciences, Tehran, Iran
e-mail: homa_h_karimi7@yahoo.de

S. M. R. Noori
Departments of Medical Physics and Biomedical Engineering, School of Medicine, Tehran University of Medical Sciences, Tehran, Iran
e-mail: smrezanoori@gmail.com

E. Jafarzadehpour
Department of Optometry, School of Rehabilitation Science, Iran University of Medical Sciences, Tehran, Iran

E. Jafarzadehpour (✉)
Department of Optometry, Faculty of Rehabilitation, Iran University of Medical Sciences, Shahnazary St., Mohseni Sq., Mirdamad Blvd., Tehran, Iran
e-mail: jafarzadehpour.e@iums.ac.ir

S. Yazdani
Ophthalmic Research Center, Shahid Beheshti University of Medical Sciences, Tehran, Iran
e-mail: shahinyazdani@yahoo.com

F. Radinmehr
Department of Optometry, School of Rehabilitation Science, Iran University of Medical Sciences, Tehran, Iran
e-mail: radinmehr_opt@yahoo.com

were extracted. Signals were reconstructed by inverse DWT. All data obtained by TD and DWT analyses were compared between the two groups.

Results In both check sizes, a significant attenuation of N95 amplitude was seen in the patient group. The relative energy of a7 of db8 increased significantly in the POAG group in the 0.8° check size. In larger check stimuli, the relative energy of d7 of coif5 decreased significantly and the standard deviation of d7 of sym7 increased markedly in glaucomatous patients ($P < 0.05$). In small stimuli, N95 descriptor (7N) of db8 had the highest value and showed a significant increase as compared to the POAG group. In the 16° check size, there was no significant difference. A strong correlation was seen between reconstructed signals and originals ($r = 0.99$).

Conclusion The DWT can quantify PERG responses more accurately. In agreement with TD and wavelet coefficients domain results, 7N of db8 decomposition can be used as a good indicator for early detection of POAG.

Keywords Primary open-angle glaucoma (POAG) · Pattern electroretinography · Discrete wavelet transforms (DWT) · Wavelet analysis

Introduction

POAG

Glaucoma, which is the main cause of irreversible blindness in the world [1], is caused by progressive destruction of axons in the optic nerve and retinal ganglion cell death [2]. The most common type of glaucoma is primary open-angle glaucoma (POAG) which is considered a group of chronic, bilateral, and asymmetric ocular disorders in adults that results in progressive optic neuropathy (morphological changes at retinal nerve fiber layer and optic disk) and visual field defects in the absence of other ocular or systemic anomalies [3]. POAG is seen in about 74% of the people with glaucoma. In a review study in 2015, the global number of patients with POAG was estimated 57.5 million cases. It is estimated that this number will increase to 65.4 million in 2020 as a result of an aging population [4]. One of the major factors causing visual impairment in glaucoma is late diagnosis of the disease [5, 6]. Therefore, early detection through the development of more reliable and precise detection methods is necessary for preventing irreversible damages [3, 7].

Open-angle glaucoma (OAG) may be diagnosed according to the three factors: intraocular pressure (IOP), pathological changes in optic disk, and specific pattern changes in visual field examination [8]. Gold standard for IOP measurement is Goldmann applanation test, but in some kind of glaucoma, such as normal tension glaucoma and in specific time in a day, the IOP is not very informative [8, 9]. However, retinal imaging such as optical coherence tomography (OCT) may be a powerful device for categorizing the retinal deformation especially in the optical disk region [10]. Different algorithms and protocols may exist in different OCT machines [11, 12]. In the best situation, OCT may reveal the structural changes that are happened due to glaucoma, but we need essential to interfere before any irreversible changes in retina; OCT is unreliable for creating applicable and timely treatment choices in early glaucoma, particularly those glaucoma patients without apparent abnormalities or conflicted test results.

Therefore, functional test may be more important. Visual field test may be a powerful and important diagnostic tool for glaucoma, but it is subjective and depends on the patient cooperation and understanding about the test [8, 13, 14]. Objective functional test for early detection of glaucoma may be more desirable [6, 15]. Electrophysiological visual test, such as visual evoked potential (VEP) and electroretinogram (ERG), is objective functional test for optic nerve, visual pathway, and retina [6, 15–17]. The pattern electroretinography (PERG) can be used to assess the performance of retinal ganglion cells and other outer retinal structural damages [6, 15, 18]. Moreover, it can improve the ophthalmologist's capability to identify early visual function loss associated with anomalies in the RGC in glaucoma subjects.

The PERG is the eye's electrophysiological responses to reverse black and white checkerboard patterns or gratings which are recorded by a corneal contact lens from the human retina [19, 20]. Transient PERG is recordable at low frequencies of checkerboard reversal (< 3 Hz) and includes an initial large positive component (P50) (45–60 ms) and a large negative component (N95) (90–100 ms) [6, 20, 21].

According to the ISCEV (International Society for Clinical Electrophysiology of Vision) protocol, PERG records are evaluated based on the amplitude and latency of P50 and N95 [20]. Since the check size affects the PERG, in early detection of glaucoma using the PERG, the PERG ratio, defined as the N95 amplitude in response to 0.8° check divided by the N95 amplitude in response to 16° check, is also measured. [13]. Due to the PERG generators, optic nerve diseases decrease N95, while P50 reduces in macular degeneration [22].

However, exact peak localization is very difficult in many cases [19]. It is shown that some glaucomatous cases had normal PERG, i.e., normal N95 amplitude and the PERG ratio [23]. Thus, PERG analysis in time domain is not precise. These disadvantages affect the validity of this valuable electrophysiological test. Hence, it is necessary to find out the specific features of the PERG for more reliable and accurate differentiation between normal and abnormal subjects.

The wavelet transforms (WT), as a powerful and capable time–frequency method in biosignals analysis, denoising, and compressing, have two forms: continuous wavelet transforms (CWT) and discrete wavelet transforms (DWT) [24–27]. This method has been applied for multi-domain processing of biosignals such as electromyogram (EMG), electroencephalogram (EEG), and electrocardiogram (ECG), but it is rarely used in vision biosignals [24]. So far, electroretinogram signals (ERG), multifocal electroretinogram (mfERG), and PERG have been analyzed using the wavelet transform [27–37].

In a study by Rogala et al. on DWT, normal and glaucomatous PERG signals were analyzed using the Daubechies mother wavelet. The DWT features were shown to be more effective than traditional time domain features in separating normal and pathological PERG waveforms using the k-means clustering algorithm [27]. The DWT allows extraction of more components and new descriptors of ERG waveforms rather than time domain and CWT; thus, time domain analysis of the retinal function should be complemented by DWT descriptors, especially in challenging diagnoses [28–30]. Discrete wavelet decomposition of mfERG in time windows provided markers for detection of glaucoma [32]. Investigations have showed that reconstruction of mfERG in different frequency bands is more sensitive than the Humphrey visual field test [34], and packet wavelet decomposition of mfERG which leads to new markers is more reliable than automate perimetry [35]. Wavelet analysis of the ERG waveforms proposed the electroretinographic index (ERI) from entropy parameters which is useful for distinguishing normal from pathological cases [38].

The PERG components may differentiate normal from pathologic signals and may be used for early detection of glaucoma [26, 27]. In this article, by evaluation of approximation and detail coefficients and scalograms of different algorithms, we focused on finding the features and descriptors of the DWT of the PERG which may help with more precise early detection of glaucoma.

Method

This study included 30 eyes of 15 patients with early POAG who were aged from 22 to 63 years (mean ± SD, 46.97 ± 13.3 years) and 30 age-matched healthy eyes.

All participants had to have best-corrected visual acuity (BCVA) of ≥ 20/30. They were categorized as normal and POAG groups. The inclusion criteria for normal individuals were normal optic disk looking, IOP < 21 mmHg, and normal 24-2 Swedish interactive threshold algorithm (SITA) standard achromatic perimetry (SAP). POAG patients were diagnosed by an open angle in gonioscopy, a glaucomatous optic nerve change associated with visual field defect in the presence of two or three following criteria: outside normal limits (ONL) glaucoma hemifield test (GHT), pattern standard deviation (PSD) probability less than 5%, and a cluster of three points on the pattern deviation plot with *P* values less than 5% including one point with *P* value less than 1%. Eyes with closed-angle glaucoma, advanced visual field loss, high myopia (> 5D), unreliable visual field data (fixation losses > 33%, false positive and false negative > 20%), ocular or systemic abnormalities such as diabetes mellitus, previous intraocular surgery (except for any uncomplicated cataract or strabismus surgery) were excluded.

Comprehensive ophthalmic tests, including BCVA measurement, dry refraction, determination of IOP with Goldmann applanation tonometry, pachymetry, slit-lamp biomicroscopy, gonioscopy, dilated fundus examination, OCT, SAP (Humphrey field analyzer

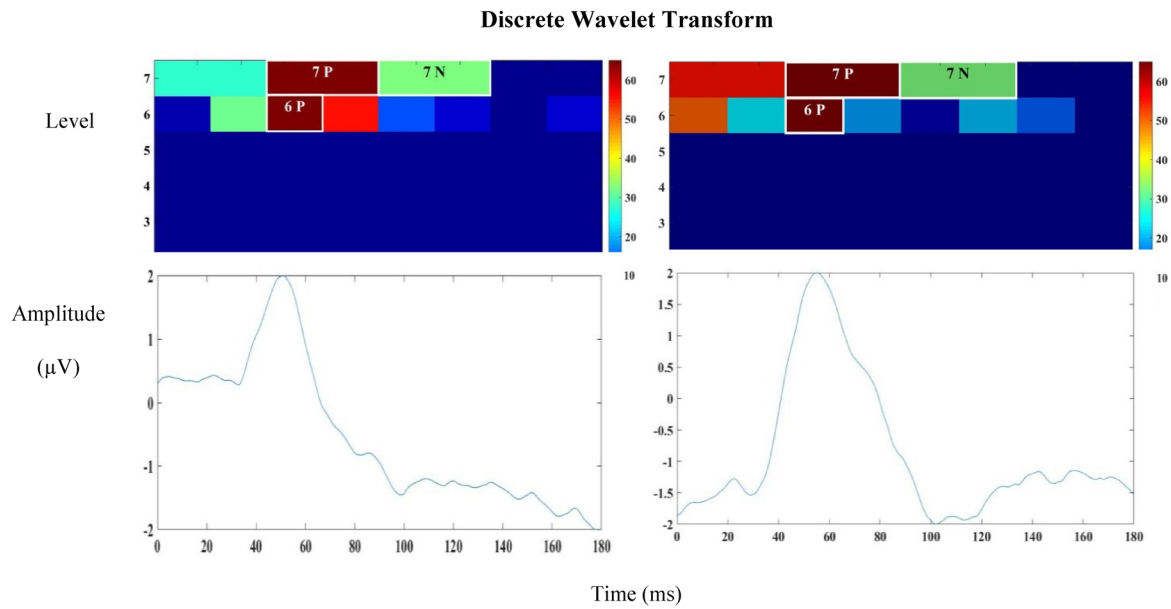

Fig. 1 Descriptors extracted from the DWT scalograms. Right: 0.8° check size, db4 scalogram and left: 16°stimuli, sym7 scalogram. 7P and 7N in level 7 and 6P in level 6 (regions with white borders) include a single wavelet coefficient and equal to energy percentage of single wavelet coefficient to total level energy. A jet color map is used in which the darkest red color corresponds to maximal energy (high wavelet coefficients) and the darkest blue color denotes minimal energy (color bars placed on the right-hand side of each scalogram)

750, SITA 24-2, Carl Zeiss Meditec, Dublin, CA, USA), were performed for all participants.

Considering the ISCEV protocol, the transient PERG responses in both groups were evaluated by the Retiport System (Roland Consult Company, Germany) in response to 0.8° and 16° black and white checkerboard stimuli with a constant mean luminance of 120 cd/m^2, contrast of 99%, and temporal frequency of 4 Hz and were stored at a sampling frequency of 2839 Hz using 512 samples. Figure 1 shows the recorded normal and abnormal PERG in the time domain.

In order to perform time–frequency domain analysis, data were transported to the MATLAB software (MATLAB R2015b). After measuring the amplitudes and latencies in the time domain, normalization and discrete wavelet transform were carried out using the Wavelet Toolbox.

Wavelet transform is one of the most useful analysis methods for signal dynamic extraction. Wavelet is just like a multilevel magnifier and helps us to recognize events with different sizes and time occurrences. This is what we need to characterize PERG for optimizing the diagnosis of early primary open-angle glaucoma (POAG).

Discrete wavelet transform (DWT) is an efficient method introduced by Mallat which is performed dyadically. Thus, the scale a and translation b are integers in the power of 2 and can be discrete as follows:

$$T_{m,n} = \int_{-\infty}^{+\infty} x(t)2^{-m/2}\Psi(2^{-m}t - n)\mathrm{d}t$$

where $T_{m,n}$ denotes localized wavelet coefficients in the discrete scale m (frequency) and discrete moment n (time), $x(t)$ represents the original signal in the time domain, and Ψ designates the wavelet function [38, 39].

After a full decomposition, the energy content of the coefficients at each scale is computed by:

$$E_m = \sum_{n=0}^{2^{M-m}-1} \left(T_{m,n}\right)^2$$

where $T_{m,n}$ is discrete wavelet transform, m is the scale integer, and n controls wavelet translation. Summation of squared detail coefficients and the square of the remaining approximation coefficients ($S_{M,0}$) is equal to the total energy of the input signal, as follows [29]:

$$E = \left(S_{M,0}\right)^2 + \sum_{m=1}^{M} \sum_{n=0}^{2^{M-m}-1} \left(T_{m,n}\right)^2$$

In the present study, in order to compare signals in different subjects before implementing wavelet transform, all signals were normalized as follows:

$$X_{i,-2 \text{ to } +2} = 2\frac{X_i - \frac{1}{2}(X_{\max} + X_{\min})}{\frac{1}{2}(X_{\max} - X_{\min})}$$

where X_i is $-i$th input, $X_{\min}$ represents the minimum input, $X_{\max}$ is the maximum input, and $X_{i,-2 \text{ to } +2}$ denotes the normalized data between -2 and $+2$.

Wavelet functions essayed to analyze the PERG waveforms were db4, db8, sym5, sym7, and coif5. Since frequencies covered by levels 1, 2, 3, 4, and 5 were higher than the PERG frequencies, the coefficients of these bands were discarded in all cases. The mean value, standard deviation, and relative energy of d6, d7, and a7 of all the above wavelets were extracted.

Scalogram of DWT is a method for local time–frequency energy visualization of input signal. It gives remarkable information about the behavior of patterns existing on signals over time changes. The DWT scalogram is represented by three axes, i.e., axis X (time), axis Y (frequency or scale), and axis Z (wavelet coefficient value or energy), represented by different colors. Deep dark red rectangles indicate high energy components (higher wavelet coefficients) of the DWT scalogram, and the blue scale denotes low energy components. Time intervals and frequency of signal components and energy distribution of wavelet coefficients can be identified by scalogram analysis [28, 29, 33, 36].

We calculated the energy percentage of a single wavelet coefficient to the total energy level in predetermined time intervals in levels 6 and 7 (low frequency) for all above-mentioned wavelets for both stimuli. With respect to the results of components extracted from the DWT scalograms of normal waveforms, normal and abnormal groups were compared only for wavelets with the highest energy. Finally, signal reconstruction was done with level 6 and summation of level 6 and 7 coefficients using wavelets with the maximum value of descriptors.

After assessment of the normal distribution of the data of time domain, coefficients domain, and DWT descriptors using the SPSS 22 software, the data were compared between normal and patient groups by Mann–Whitney test. Finally, Spearman correlation coefficients were used in order to compare the similarities between reconstructed signals and PERG waveforms.

Results

Results obtained in time domain analysis (Table 1a) showed a significant reduction in N95 amplitude in

Table 1 a) Meaningful results of comparison of mean value of amplitudes and latencies between normal and abnormal signals in time domain analysis, b) meaningful results of comparison of mean value, standard deviation, and relative energy of d6, d7, and a7 of DWT of the PERG waveforms

	Patient (mean ± SD)	Normal (mean ± SD)	*P* value	
a)				
N95 amplitude (μV)	9.78 ± 2.50	11.11 ± 2.62	0.047	S B–W
N95 amplitude (μV)	8.78 ± 3.10	11.68 ± 3.95	0.012	L B–W

	Patient (mean ± SD)	Normal (mean ± SD)	Frequency range (Hz)	*P* value	Wavelet	
b)						
%(E_a7* /Et)	8.68% ± 0.016	7.30% ± 0.035	0–11.08	0.036	db8	S B–W
%(E_d7** /Et)	2.80% ± 0.0070	3.18% ± 0.0066	11.08–22.17	0.049	coif5	L B–W
STD_d7***	0.9555 ± 0.0300	0.9314 ± 0.0248	11.08–22.17	0.026	sym5	L B–W

E_t total energy, *S B–W* Small (0.8°) Black–White check size, *L B–W* Large (16°) Black–White check size

*E_a7: Energy of approximation coefficients level 7

** E_d7: Energy of detail coefficients level 7

***STD d7: Standard Deviation of detail coefficients level 7

both stimuli ($P < 0.05$). However, there was no statistically significant difference in N95 latency and also implicit time and amplitude of P50 ($P > 0.1$).

In the present study, the mean value and standard deviation of d6, d7, and a7 and also the percentage of the relative energy of these coefficients obtained by the DWT of the mentioned wavelets of the PERG signals in both normal and POAG subjects in response to 0.8° and 16° stimuli were compared. Table 1b shows significant differences of these comparisons. As shown in Table 1b, comparison of the mean value of detail coefficients in both stimuli showed no significant difference between healthy and glaucomatous subjects. In smaller stimuli, the a7 relative energy of db8 wavelet was considerably higher in patients than controls.

In the 16° check size, the d7 relative energy of coif5 wavelet decreased significantly in POAG patients; in addition, the d7 standard deviation of sym5 wavelet in normal eyes showed a marked increase ($P < 0.05$).

As shown in Fig. 1, the DWT scalograms of PERG signals decomposed them into seven frequency bands. Scalogram analysis facilitates selection of coefficients related to peaks. In both stimuli, three major frequency components (6P, 7P, 7N) were identified in the time–frequency domain (Fig. 1). In small stimuli, the DWT of healthy signals showed that the energy percentage of P50 in level 6 (P6) in sym7, db4, coif5, db8, and sym5 wavelets was 64.88% ± 10.01, 61.88% ± 20.27, 45.17% ± 20.88, 39.03% ± 17.31, and 29.51% ± 10.07, respectively. Descriptor of P50 in level 7 (7P) had a maximum value in sym7 analysis, and its values in db4, sym5, db8, and coif5 were 50.78% ± 11.61, 41.16% ± 14.71, 11.19% ± 5.41, and 5.31% ± 3.56, respectively. The energy percentage of N95 (7N) was much lower than P50 and could only be separated in level 7. Db8 showed the highest amount of 7N among wavelets. 7N was 7.90% ± 5.79 for db4, 2.88% ± 2.33 for sym7, 2.48% ± 2.42 for sym5, and 0.45% ± 0.43 for coif5. In large stimuli, 6P and 7P had their highest values in sym5, followed by sym7 with 34.86% ± 23.54 (6P) and 49.11% ± 16.77 (7P). 7N showed the maximum value in sym7 followed by db4 (7.84% ± 4.58).

Table 2 shows the results of the comparison of descriptors between healthy and patient groups. The results revealed that 6P and 7P could not discriminate normal from abnormal signals. The only considerable difference was seen in 7N obtained by db8 analysis in small check (Fig. 2) ($P < 0.05$). These results are in agreement with time domain and coefficients domain results.

Applying inverse DWT, signal reconstruction was performed by summating level 6 and 7 coefficients using sym7 in 0.8° and sym5 in 16° check size. Figure 3 represents reconstructed signals. Spearman analysis showed a strong ($r = 0.99$) significant correlation ($P < 0.000$) between the original signal and the reconstructed one.

Discussion

The PERG can reveal trivial changes in electrical activities of retinal ganglion cells. However, since the

Table 2 a) Results of comparison of extracted descriptors of P50 (6P, 7P) from sym7 scalogram analysis and main component of N95 (7N) by db8 scalogram analysis for 0.8° stimuli, b) results of comparison of extracted components of P50 (6P, 7P) from sym5 scalogram analysis, and main component of N95 (7N) by sym7 scalogram analysis for 16° stimuli

Descriptor	Frequency band (Hz)	Time interval (ms)	Patient (mean ± SD)	Normal (mean ± SD)	*P* value
a)					
6P	44.35–22.17	45–67.5	65.05% ± 14.96	64.88% ± 10.01	0.961
7P	11.08–22.17	45–90	87.80% ± 9.47	85.36% ± 11.03	0.365
7N	11.08–22.17	90–135	11.71% ± 4.66	8.89% ± 4.17	**0.020***
b)					
6P	44.35–22.17	45–67.5	40.95% ± 10.94	37.51% ± 9.59	0.32
7P	11.08–22.17	45–90	73.89% ± 10.91	72.79% ± 19.80	0.68
7N	11.08–22.17	90–135	8.32%± 4.69	9.98% ± 5.22	0.22

*Statistically significant difference from normal control

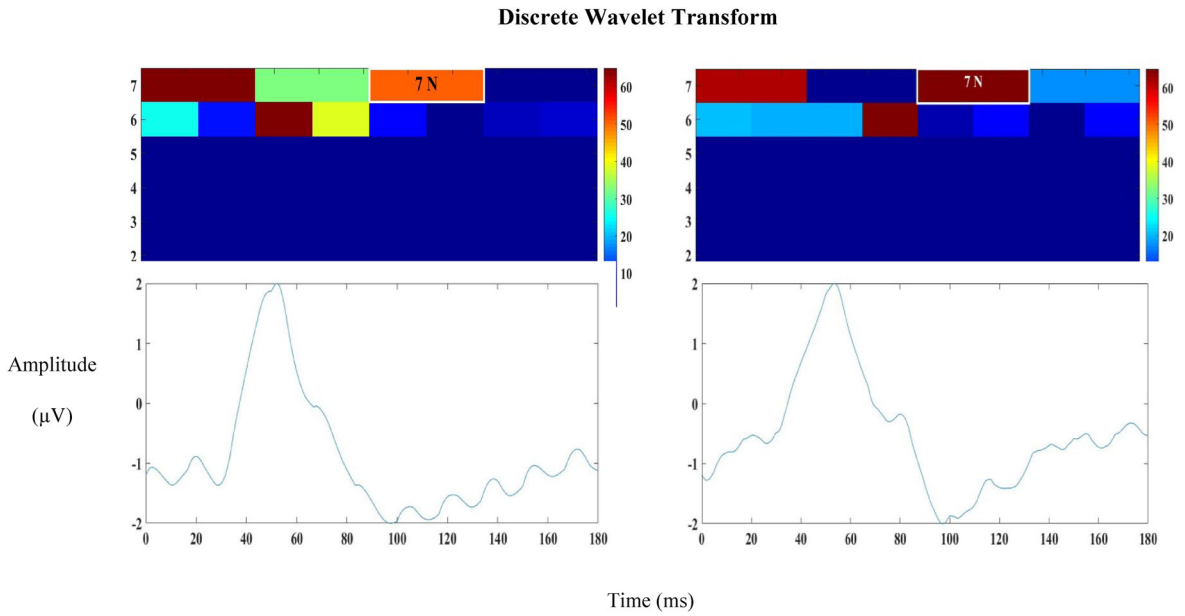

Fig. 2 Meaningful difference of 7N between healthy and pathological small stimuli signals extracted from DWT scalograms using db8 (right: normal, left: patient). Deep dark red rectangles show higher energy components (high wavelet coefficients) of the DWT scalogram and blue ones denote low energy (color bars placed on the right-hand side of each scalogram)

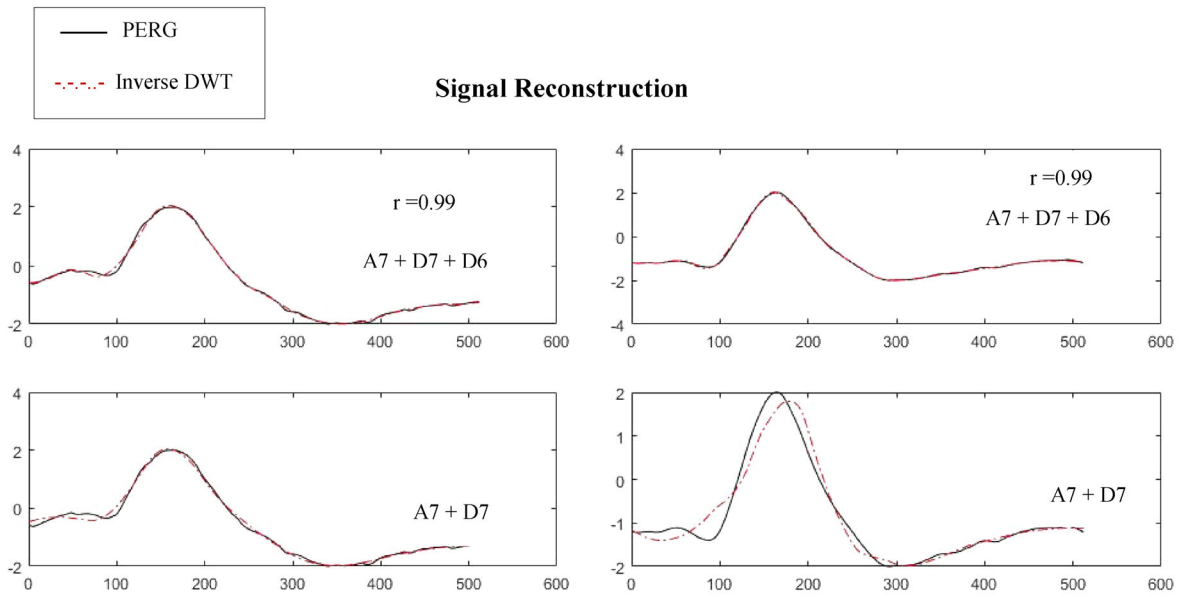

Fig. 3 Reconstructed signal by sym7 (left: small stimuli) and sym5 (right: large stimuli)

PERG is a global response and many recorded signals are affected by various factors, these changes may be too small in disease conditions to be detected. The traditional methods of measuring signal parameters may lead to considerable errors in many cases and precise peak localization is difficult [19]. In this paper, in order to find features which help to localize the peaks more precisely and to improve early diagnosis,

we performed the DWT of the PERG signals of POAG patients and normal subjects. So far, only Rogala and Brykalski [27] have used discrete wavelet transform to review the PERG waveforms. They suggested a new method of preprocessing of PERG signals. Comparison of normal and glaucomatous PERG waveforms using the DWT showed that the DWT features were more effective than traditional time domain ones in differentiating normal and pathological PERG waveforms using the k-means clustering algorithm. Moreover, the misclassification rate ranges from 55 to 60% for traditional time domain parameters and 34–36% for the DWT [27].

In agreement with previous investigations which showed the glaucomatous PERG amplitude was significantly lower than normal [13, 40–45], the results of time domain analysis in both checks (Table 1a) in this study also showed a marked reduction in N95 amplitude in eyes with glaucoma. However, the amplitude and latency of P50 peak in both checks had no significant changes in the patient group. Jafarzadehpur et al. showed that the N95 amplitude decreased in primary open-angle glaucoma, whereas the amplitude and implicit time of P50 showed no observable changes [43]. Demir et al. demonstrated that N95 amplitude reduction is greater than P50 amplitude, and these reductions are in agreement with retinal neuronal fiber layer (RNFL) thinning that are evaluated by OCT and are correlated with visual field sensitivity loss in POAG patients [44]. Parisi et al. found significant correlations between N95 amplitude and RNFL thickness in OAG eyes only by using 15′ (0.25°) check size in glaucomatous eyes. Moreover, the RNFL values correlated well with corrected pattern standard deviation HFA in these patients [17]. The decrease in N95 amplitude was reported in open-angle glaucoma which showed significant correlations with Humphrey field analyzer 24-2 mean deviation (HFA 24-2 MD). It has been offered that in OAG eyes, the PERG N95 amplitude reduction may indicate impairment in the function of the innermost retinal layers [16]. Moreover, N95 originates from ganglion cells and its amplitude may measure ganglion cells population indirectly, and a reduction in its amplitude correlates with the severity of glaucoma [44].

The main concern in wavelet decomposition is selection of appropriate mother wavelet, because computing wavelet coefficients directly depend on the mother wavelet function shape [46]. In 2005, Rogala et al. compressed the PERG signals using different wavelets and substituted fourth level approximation for original signal. They ultimately compared the compression efficiency of different wavelets [27]. Therefore, db4, db8, sym5, sym7, and coif5 wavelets, which had higher efficiency, were used in this study.

As shown in Table 1b, the relative energy of a7 in db8 was 8.68% ± 0.016 in the glaucomatous group and 7.30% ± 0.035 in the normal group. This significant increase ($P < 0.05$) may indicate the retinal mechanism disruption and neuronal pathways alteration due to the disease. Sunga and Enoch assessed the visual field of glaucoma patients using a method described by Westheimer and found out that lateral inhibition in normal areas was more than scotoma and hypothesized that the reduction in glaucoma was a result of the retrograde damage of synapses involved in this process [46]. Montolio et al. compared lateral inhibition between normal and glaucoma subjects, and the results showed retrograde reduction in lateral inhibition [47]. On the other hand, the excitotoxicity hypothesis states that in POAG, glutamate released from postsynaptic neurons stimulates ionotropic receptors on postsynaptic neurons (RGCs) and causes excitatory postsynaptic currents and activation of voltage-gated calcium channels [48, 49]. Thus, it is very probable that increased energy of a7 in the frequency range of N95 is related to decrease lateral inhibition and increased postsynaptic current. However, the amplitude may increase or decrease in a specific peak, but the energy that is distributed in a specific window may decrease or increase despite the peak in the specific window.

The results of this study showed amplitude reduction in time domain, whereas the relative energy increased in the time–frequency domain. It can be proposed that the amplitude decreases because of localized reduction in neurons, while the energy increases due to attribution of different neurons. "Amplitude is not additive along the frequency axis" [50], indicating that if you record an electrophysiological signal, the peaks and troughs show specific cell responses. However, in disease situations, the cells do not respond normally and lateral inhibition does not occur as in normal cells; therefore, some cells are not inhibited. However, in the time–frequency domain and in the DWT, "the total power in the frequency domain is obtained by integration over the frequency

range" [50]. Therefore, integrated responses of the cells, which are partly inhibited in normal subjects, may lead to an augmentation in the relative energy.

The results of signal analysis using coif5 showed a marked decline in the relative energy of d7 in larger stimuli ($P < 0.05$). According to the frequency range of this band which contains both P50 and N95 peaks, energy reduction may indicate that the existing cells have poorer responses to 16° stimuli in patients with POAG.

The considerable increase in d7 standard deviation of sym5 wavelet in glaucoma subjects may demonstrate dedicative cell operation in normal subjects and variety in activated cells and more undedicated cell function in the glaucoma group (Table 1). The nonspecific function of some cells leads to similar results in both normal and patient groups in the time domain, time–frequency, and frequency domain. This point can be confirmed by increased variance.

In both 0.8° and 16° stimuli, the P50 and N95 peaks were determined in DWT scalograms (Fig. 1) by distinct components located in the level 6 (6P descriptor) at 22.17 Hz and in the level 7 (7P and 7N descriptors) at 11.08 Hz. These descriptors included a single wavelet coefficient. Gauvin et al. used the DWT scalograms of the photopic ERG signal to identify descriptors which characterized a-wave, b-wave, and Ops in temporal windows and frequency bands [28]. Their novel DWT descriptors for 20a, 40a, and 20b comprised a single wavelet coefficient in levels 6 and 7 (i.e., rectangle), while other descriptors included several coefficients [28, 29]. Their results showed that the ERG analysis was more complete in the time–frequency domain, and the DWT descriptors could be used as a complement to time domain analysis of the ERG [28, 29]. In 2017, Gauvin et al. showed that the DWT descriptors offered a rapid and easy approach for determination of ON and OFF pathways in short-flash ERGs [37]. Miguel et al. identified markers for detection of glaucoma by discrete wavelet transform of mfERG in time windows [32]. In 2010, they used the DWT decomposition to reconstruct mfERG signals and indicated higher sensitivity of this method as compared to the Humphrey visual field test to detect the changes in eyes with glaucoma [34].

In the present study, in analysis of normal signals of the small check, sym7 and db4 showed higher descriptor values of P50 and db8 could extract the N95 descriptor better than others. It could be stated that among five wavelets, these wavelet functions were more efficient in characterizing and evaluating P50 and N95 peaks. The results given in Table 2a indicate that 7N descriptor can only discriminate normal signals from patient signals which are in line with the results of time domain and level 7 approximation coefficients. Hence, the 7N descriptor derived from db8 in 0.8° check size corresponds to the N95 peak. Therefore, N95 and 7N descriptor can be used for early diagnosis of POAG. The differences between the two groups were very subtle, which may be due to the fact that our cases were very borderline (almost normal).

In 16° stimuli, higher amounts of 6P and 7P obtained by sym5 analysis of normal waveforms and maximum value of 7N in sym7 analysis showed the efficacy of these two wavelet functions among other wavelets to identify the main components of the PERG. However, there was no significant discrepancy between control and patient groups. The obtained results are in agreement with time domain results and also previous studies, demonstrating the higher sensitivity of 0.8° check size to glaucomatous ganglion cell damage as compared to larger checks such as 16° [13, 40, 51].

The wavelet transform is a successful and valuable approach for analyzing biosignals. Investigations have shown that WT of the PERG waveforms can define amplitude parameters with improved accuracy, stability, and reliability as compared to conventional methods. DWT features suggest better separability between normal and pathological PERG in contrast to traditional time domain features [26, 27]. Therefore, discrete wavelet transform of the PERG can be performed to identify new features which help to distinguish between normal and abnormal signals and make a more precise and reliable diagnosis. The DWT scalograms can localize major components of PERG more precisely and extract them in time intervals and frequency bands, leading to early detection of glaucoma. In the present study, although 7N descriptor extracted from db8 scalogram and some of the relative energy and energy percentages had significant differences between patient and control groups, changes were very small and hard to appreciate clinically given the low effect size. Larger datasets and more samples are needed to confirm the accuracy of the results.

Compliance with ethical standards

Conflict of interest All authors certify that there is no actual or potential conflict of interest in relation to this article.

Ethical approval All procedures performed in studies involving human participants were in accordance with the ethical standards of the institutional and/or national research committee and with the 1964 Declaration of Helsinki and its later amendments or comparable ethical standards.

Informed consent Informed consent was obtained from all individual participants included in the study.

References

1. Schon K, Wollstein G, Schuman JS, Sung KR (2014) Prediction of glaucomatous field progression: pointwise analysis. Curr Eye Res 39:705–710
2. Johnson EC, Morrison JC (2009) Friend or foe? Resolving the impact of glial response in glaucoma. J Glaucoma 18(5):341–353. https://doi.org/10.1097/IJG.0b013e31818c6ef6
3. Weinreb RN, Khaw PT (2004) Primary open-angle glaucoma. Lancet 363(9422):1711–1720. https://doi.org/10.1016/S0140-6736(04)16257-0
4. Kapetanakis VV, Chan MP, Foster PJ, Cook DG, Owen CG, Rudnicka AR (2015) Global variations and time trends in the prevalence of primary open angle glaucoma (POAG): a systematic review and meta-analysis. Br J Ophthalmol 100(1):86–93. https://doi.org/10.1136/bjophthalmol-2015-307223
5. Bettin P, Di Matteo F (2013) Glaucoma: present challenges and future trends. Ophthalmic Res 50:197–208
6. Weinreb RN, Aung T, Medeiros FA (2014) The pathophysiology and treatment of glaucoma: a review. JAMA 311(18):1901–1911. https://doi.org/10.1001/jama.2014.3192
7. Kreuz AC, Oyamada MK, Hatanaka M, Monteiro MLR (2014) The role of pattern-reversal electroretinography in the diagnosis of glaucoma. Arq Bras Oftalmol 77(6):403–410. https://doi.org/10.5935/0004-2749.20140101
8. Omoti AE, Okeigbemen VW, Waziri-Erameh JM (2009) Current concepts in the diagnosis of primary open angle glaucoma. West Afr J Med 28(3):141–147
9. Takagi D, Sawada A, Yamamoto T (2017) Evaluation of a new rebound self-tonometer, Icare homa: comparison with Goldman applanation tonometer. J Glaucoma 26(7):613–618. https://doi.org/10.1097/IJG.0000000000000674
10. Bussel II, Wollstein G, Schuman JS (2014) OCT for glaucoma diagnosis, screening and detection of glaucoma progression. Br J Ophthalmol 98(Suppl 2):ii15–ii19. https://doi.org/10.1136/bjophthalmol-2013-304326
11. Popescu DP, Choo-Smith LP, Flueraru C, Mao Y, Chang S, Disano J, Sherif S, Sowa MG (2011) Optical coherence tomography: functional principles, instrumental designs and biomedical applications. Biophys Rev 3(3):155–169. https://doi.org/10.1007/s12551-011-0054-7
12. Podoleanu AG (2012) Optical coherence tomography. J Microsc 247(3):209–219. https://doi.org/10.1111/j.1365-2818.2012.03619.x
13. Bach M, Hoffmann MB (2008) Update on the pattern electroretinogram in glaucoma. Optom Vis Sci 85(6):386–395. https://doi.org/10.1097/OPX.0b013e318177ebf3
14. Wu Z, Medeiros FA (2018) Recent development in visual field testing for glaucoma. Curr Opin Ophthalmol 29(2):141–146. https://doi.org/10.1097/ICU.0000000000000461
15. Leonard KC, Hutnik CML (2010) Using electroretinography for glaucoma diagnosis. In: Schacknow PN, Samples JR (eds) The glaucoma book: a practical, evidence-based approach to patient care, 1st edn. Springer, Berlin, pp 265–267
16. Parisi V, Miglior S, Manni G, Centofanti M, Bucci MG (2006) Clinical ability of pattern electroretinograms and visual evoked potentials in detecting visual dysfunction in ocular hypertension and glaucoma. Ophthalmology 113:216–228. https://doi.org/10.1016/j.ophtha.2005.10.044
17. Parisi V, Manni G, Centofanti M, Gandofi SA, Ozli D, Bucci M (2001) Correlation between optical coherence tomography, pattern electroretinogram, and visual evoked potentials in open-angle glaucoma patients. Ophthalmology 108:905–912
18. Luo X, Frishman LJ (2011) Retinal pathway origins of the pattern electroretinogram (PERG). Investig Ophthalmol Vis Sci 52(12):8571–8584. https://doi.org/10.1167/iovs.11-8376
19. Fisher AC, Hagan RP, Brown MC (2007) Automatic positioning of cursors in the transient pattern electroretinogram (PERG) with very poor SNR using an expert system. Doc Ophthalmol 115:61–68
20. Bach M, Brigell MG, Holder GE, Meigen T, Hawlina M, Johnson MA, Viswanathan S, McCulloch DL (2013) ISCEV standard for clinical pattern electroretinography (PERG): 2012 update. Doc Ophthalmol 126:1–7
21. Berninger TA, Arden GB (1988) The pattern electroretinogram. Eye (Lond) 2(Suppl):S257–S283. https://doi.org/10.1038/eye.1988.149
22. Porciatti V (2015) Electrophysiological assessment of retinal ganglion cell function. Exp Eye Res 141:164–170. https://doi.org/10.1016/j.exer.2015.05.008
23. Hood DC, Xu L, Thienprasiddhi P, Greenstein VC, Odel JG, Grippo TM, Liebmann JM, Ritch R (2005) The pattern electroretinogram in glaucoma patients with confirmed visual field deficits. Investig Ophthalmol Vis Sci 46:2411–2418. https://doi.org/10.1167/iovs.05.0238
24. Rafiee J, Rafiee MA, Prause N, Schoen MP (2011) Wavelet basis functions in biomedical signal processing. Expert Syst Appl 38(5):6190–6201. https://doi.org/10.1016/j.eswa.2010.11.050
25. Akay M (1998) Time frequency and wavelets in biomedical signal processing. IEEE Press series in Biomedical Engineering, First edn. Wiley, New York, pp 230–257
26. Penkala K (2010) Continuous wavelet transformation of pattern electroretinogram (PERG)-a tool improving the test accuracy. In: Bamidis P, Pallikarakis N (eds) XII

Mediterranean conference on medical and biological engineering and computing 2010. Springer, Berlin, pp 196–199
27. Rogala T, Brykalski A (2005) Wavelet feature space in computer-aided electroretinogram evaluation. Pattern Anal Appl 8:238–246. https://doi.org/10.1007/s10044-005-0003-9
28. Gauvin M, Lina JM, Lachapelle P (2014) Advance in ERG analysis: from peak time and amplitude to frequency, power, and energy. Biomed Res Int. https://doi.org/10.1155/2014/246096
29. Gauvin M, Little JM, Lina JM, Lachapelle P (2015) Functional decomposition of the human ERG based on the discrete wavelet transform. J Vis 15(16):1–22
30. Gauvin M, Chakor H, Koenekoop RK, Little JM, Lina JM, Lachapelle P (2016) Witnessing the first sign of retinitis pigmentosa onset in the allegedly normal eye of a case of unilateral RP: a 30-year follow-up. Doc Ophthalmol 132:213–229. https://doi.org/10.1007/s10633-016-9537-y
31. Varadharajan S, Fitzgerald K, Lakshminarayanan V (2000) Wavelet analysis of ERG of patients with Duchenne Muscular Dystrophy. In: Vision science and its application, OSA Technical Digest, pp 65–68
32. Miguel Jimenez JM, Blanco R, Boquete L, Rodriguez Ascariz JM, De la Villa Polo P (2008) Multifocal electroretinography. Glaucoma diagnosis by means of the wavelet transform. In: Electrical and computer engineering, CCEC, Canadian conference, pp 867–870
33. Varadharajan S, Fitzgerald K, Lakshminarayanan V (2007) A novel method for separating the components of the clinical electroretinogram. J Mod Opt 54(9):1263–1280
34. Miguel-Jimenez JM, Boquete L, Ortega S, Rodriguez-Ascariz JM, Blanco R (2010) Glaucoma detection by wavelet-based analysis of the global flash multifocal electroretinogram. Med Eng Phys 32:617–622
35. Miguel-Jimenez JM, Ortega S, Boquete L, Rodriguez-Ascariz JM, Blanco R (2011) Multifocal ERG wavelet packet decomposition applied to glaucoma diagnosis. BioMed Eng Online 10:37. https://doi.org/10.1186/1475-925X-10-37
36. Nair SS, Joseph P (2014) Wavelet based electroretinographic signal analysis for diagnosis. Biomed Signal Process Control 9(1):37–44. https://doi.org/10.1016/j.bspc.2013.09.008
37. Gauvin M, Suster M, Little JM, Brecelj J, Lina JM, Lachapelle P (2017) Quantifying the on and off contributions to the flash ERG with the discrete wavelet transform. Trans Vis Sci Technol 6(1):3. https://doi.org/10.1167/tvst.6.1.3
38. Mallat SG (2009) A wavelet tour of signal processing the sparse way, 3rd edn. Academic Press, Houston
39. Addison PS (2002) The illustrated wavelet transform handbook: introductory theory and applications in science, engineering, medicine and finance. CRC Press, Boca Raton. https://doi.org/10.1201/9781420033397.fmatt
40. Bode SF, Jehle T, Bach M (2011) Pattern electroretinogram (PERG) in glaucoma suspects-new findings from a longitudinal study. Investig Ophthalmol Vis Sci 52:4300–4306. https://doi.org/10.1167/iovs.10-6381
41. Graham SL, Drance SM, Chauhan BC, Swindale NV, Hnik P, Mikelberg FS, Douglas GR (1996) Comparison of psychophysical and electrophysiological testing in early glaucoma. Investig Ophthalmol Vis Sci 37:2651–2662
42. Jafarzadehpour E, Radinmehr F, Pakravan M, Mirzajani A, Yazdani SH (2013) Pattern electroretinography in glaucoma suspects and early primary open angle glaucoma. J Ophthalmic Vis Res 8(3):199–206
43. Demir ST, Oba ME, Erdogan ET, Odabasi M, Dirim AB, Demir M, Can E, Kara O, Sendül (2015) Comparison of pattern electroretinography and optical coherence tomography parameters in patients with primary open-angle glaucoma and ocular hypertension. Turk J Ophthalmol 45:229–234
44. Ventura LM, Sorokac N, Santos RDL, Feuer WJ, Porciatti V (2006) The relationship between retinal ganglion cell function and retinal nerve fiber thickness in early glaucoma. Investig Ophthalmol Vis Sci 47(9):3904–39011
45. Ganekal S, Dorairaj S, Jhanji V (2013) Pattern electroretinography changes in patients with established or suspected primary open angle glaucoma. J Curr Glaucoma Pract 7(2):39–42. https://doi.org/10.5005/jp-journal-10008-1135
46. Sunga RN, Enoch JM (1970) A static perimetric technique believed to test receptive field properties. 3. Clinical trials. Am J Ophthalmol 70:244–272
47. Junoy Montolio FG, Meems W, Janssens MSA, Stam L, Jansonius NM (2016) Lateral inhibition in the human visual system in patients with glaucoma and healthy subjects: a case control study. PLoS ONE 11(3):e0151006. https://doi.org/10.1371/journal.pone.0151006
48. Mueller BH, Stankowska DL, Krishnamoorthy PR (2011) Neuroprotection in glaucoma. In: RumeltSh (ed) Glaucoma—basic and clinical concepts. INTECH Open Access Publisher
49. Cheung W, Guo L, Cordeiro MF (2008) Neuroprotection in glaucoma: drug-based approaches. Optom Vis Sci 85(6):406–416. https://doi.org/10.1097/OPX.0b013e31817841e5
50. Van der Tweel LH, Estévez O (2006) Analytical techniques. In: Heckenlively JR, Arden GB (eds) Principles and practice of clinical electrophysiology of vision, 2nd edn. MIT Press, Cambridge, pp 439–459
51. Bach M, Speidel-Fiaux A (1989) Pattern electroretinogram in glaucoma and ocular hypertension. Doc Ophthalmol 73(2):173–181. https://doi.org/10.1007/BF00155035